ISSN 0021-3640, JETP Letters, 2018, Vol. 108, No. 3, pp. 189–195. © Pleiades Publishing, Inc., 2018.
Original Russian Text © D.M. Dzebisashvili, A.A. Khudaiberdyev, 2018, published in Pis'ma v Zhurnal Eksperimental'noi i Teoreticheskoi Fiziki, 2018, Vol. 108, No. 3, pp. 189–195.

CONDENSED MATTER

Quantum Oscillations of Magnetization in Antiferromagnetic Semimetals on a Triangular Lattice

D. M. Dzebisashvili[a, b, *] and A. A. Khudaiberdyev[a]

[a] *Kirensky Institute of Physics, Federal Research Center Krasnoyarsk Scientific Center, Siberian Branch, Russian Academy of Sciences, Krasnoyarsk, 660036 Russia*

[b] *Reshetnev Siberian State University of Science and Technology, Krasnoyarsk, 660037 Russia*

**e-mail: ddm@iph.krasn.ru*

Received June 25, 2018

The specific features of magnetization in antiferromagnetic semimetals with a low charge carrier density on a triangular lattice in a high magnetic field are studied. It is demonstrated that the well-known plateau in the magnetic field dependence of the magnetization manifesting itself in the subsystem of localized $S = 1/2$ spins is actually not strictly horizontal but has a slight positive slope. It is found that an abrupt change in the frequency of quantum oscillations of the magnetization in the itinerant subsystem should be observed at the magnetic field values corresponding to the edges of this plateau owing to the strong s–$d(f)$ exchange coupling.

DOI: 10.1134/S0021364018150067

1. INTRODUCTION

A quantum antiferromagnet on a triangular lattice (AFTL) is the simplest system most often used in the studies of geometrical frustration [1]. It is well known that the ground state of the classical AFTL is highly degenerate [2]. At zero temperature, quantum fluctuations lift the degeneracy in favor of a planar structure [3]. Quantum fluctuations are responsible for a plateau (horizontal segment) in the magnetic field dependence of the magnetization $M(H)$ at $M = M_{sat}/3$, where M_{sat} is the saturation magnetization [3, 4]. In the range of applied magnetic fields $[H_1, H_2]$, where the magnetization has a plateau, the system corresponds to the so-called *uud* phase. In this case, the magnetization vectors of two of the three magnetic sublattices are oriented along the applied magnetic field **H**, whereas the magnetization of the third sublattice is directed opposite to the field. At $H < H_1$ and $H > H_2$, the system is in the Y and V phases, respectively. The plateau in the magnetic field dependence was observed in experiments with several quasi-two-dimensional AFTL compounds such as $GdPd_2Al_3$ [5], $RbFe(MoO_4)_2$ [6, 7], $Ba_3CoSb_2O_9$ [8], and $Rb_4Mn(MoO_4)_3$ [9].

Currently, compounds in which the specific features of the AFTL magnetic structure manifest themselves in the characteristics of the subsystem of itinerant electrons attract great interest. A prominent example of such compounds is provided by water-intercalated $Na_xCoO_2 \cdot H_2O$ sodium cobaltites whose conducting layers form a triangular lattice. The interplay between the localized and itinerant degrees of freedom in the phase of coexisting superconductivity and long-range magnetic order in this system was actively discussed in [10–14].

Other examples of conducting AFTLs are $PdCrO_2$, $AgNiO_2$, and Ag_2CrO_2 (see [15] and references therein). These systems are also characterized by the strong coupling between conduction electrons and localized spins. Note in this connection that the s–$d(f)$ exchange interaction in these antiferromagnetic semimetals with the cubic and square crystal lattices can lead to the drastic change in the frequency of quantum oscillations of magnetization for the subsystem of itinerant charge carriers near the magnetic field corresponding to the spin-flip transition [16, 17].

In this work, we study the possibility of observing the anomalies of quantum oscillations in antiferromagnetic semimetals on the triangular lattice close to the fields H_1 and H_2 determining the magnetization plateau for the localized spins. To this end, we develop the theory of quantum AFTLs with $S = 1/2$ based on the spin diagram technique for the Matsubara Green's functions. Then, in the framework of the Lifshitz–Kosevich theory, we analyze the specific features of the quantum oscillations of magnetization for charge carriers in AFTL semimetals with strong coupling between the spin and charge degrees of freedom. Here, an important condition is the low charge carrier density, which in the main approximation allows us to neglect the effect of charge carriers on the subsystem of localized spins.

2. HAMILTONIAN OF THE QUANTUM ANTIFERROMAGNET ON THE TRIANGULAR LATTICE. EQUATIONS FOR ANGLES

Let us discuss a set of triangular lattices with spins $S = 1/2$ located at the lattice sites. Using these lattices, we form a simple hexagonal lattice. We take into account the exchange interaction only between the nearest neighbor spins: an antiferromagnetic one between the spins of any triangular lattice and a weak ferromagnetic one between the spins of different lattices. The Hamiltonian of this system can be written in the form

$$\mathcal{H}_m = \sum_{\langle ij \rangle} I_{ij} \mathbf{S}_i \mathbf{S}_j + gH \sum_j S_j^z. \quad (1)$$

Here, $\mathbf{S}_j$ is the vector operator for the spin localized at the jth site, H is the strength of the applied magnetic field directed along the z axis and measured in energy units, g is the Landé g-factor, I_{ij} is the exchange interaction energy of the spins located at the ith and jth sites ($I_{ij} = I > 0$ for the nearest neighbor sites within one triangular lattice and $I_{ij} = I_\perp < 0$ for the sites from different lattices). We assume that $I \gg |I_\perp|$. For all other pairs of spins, $I_{ij} = 0$. The angular brackets in the first sum denote the summation over the nearest neighbor sites.

To describe the canting of magnetization vectors in the applied magnetic field, we divide the system into three magnetic sublattices and pass to the local coordinate system in each of them. The new axes are rotated by angles θ_l ($l = 1, 2, 3$) with respect to the initial ones (see Fig. 1). Such rotation corresponds to the unitary transformation for all A operators: $A \to A' = \hat{U} A \hat{U}^+$, where $\hat{U} = \prod_{l=1}^{3} \prod_{f_l} \exp\{i\theta_l S_{f_l}^y\}$, and subscript f_l spans over all angles in the lth sublattice. For the spin operators, we find

$$\begin{aligned} S_{f_l}^x(\theta_l) &= S_{f_l}^x \cos\theta_l + S_{f_l}^z \sin\theta_l, \quad S_{f_l}^y(\theta_l) = S_{f_l}^y, \\ S_{f_l}^z(\theta_l) &= S_{f_l}^z \cos\theta_l - S_{f_l}^x \sin\theta_l \quad (l = 1, 2, 3). \end{aligned} \quad (2)$$

After passing to the local coordinate systems and separating out the mean-field contributions, it is convenient to represent Hamiltonian (1) in the form

$$\mathcal{H}'_m = \mathcal{H}_0 + \mathcal{H}_{\text{int}}, \quad (3)$$

where

$$\mathcal{H}_0 = \sum_{l=1}^{3} \sum_{f_l} H_l S_{f_l}^z + E_0, \quad (4)$$

$$H_l = 3I(R_{l+1} \cos\theta_{l,l+1} + R_{l+2} \cos\theta_{l+2,l}) - gH \cos\theta_l + 4I_\perp R_l,$$

$$E_0 = -N \sum_{l=1}^{3} \left(3I R_l R_{l+1} \cos\theta_{l,l+1} + 2I_\perp R_l^2 \right),$$

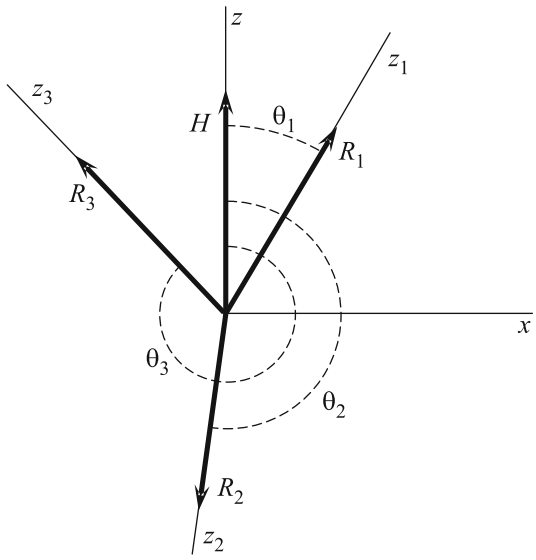

Fig. 1. Orientations of the local axes z_l ($l = 1, 2, 3$) and equilibrium sublattice magnetizations $\mathbf{R}_l$ after the rotation of the local coordinate systems by the angles θ_l about the y axis.

$$\begin{aligned} \mathcal{H}_{\text{int}} = I \sum_{l=1}^{3} \sum_{f_l} \Big[& \Delta S_{f_l}^z \Delta S_{f_{l+1}}^z \cos\theta_{l,l+1} \\ & + \frac{1}{4}(\cos\theta_{l,l+1} - 1)\left(S_{f_l}^+ S_{f_{l+1}}^+ + S_{f_l}^- S_{f_{l+1}}^- \right) \\ & + \frac{1}{4}(\cos\theta_{l,l+1} + 1)\left(S_{f_l}^+ S_{f_{l+1}}^- + S_{f_l}^- S_{f_{l+1}}^+ \right) \\ & + \sin\theta_{l,l+1}\left(\Delta S_{f_l}^z S_{f_{l+1}}^x - S_{f_l}^x \Delta S_{f_{l+1}}^z \right) \Big] \\ & + I_\perp \sum_{l=1}^{3} \sum_{\langle f_l f'_l \rangle} \left[S_{f_l}^+ S_{f'_l}^- + \Delta S_{f_l}^z \Delta S_{f'_l}^z \right]. \end{aligned} \quad (5)$$

Here, $R_l = \langle S_{f_l}^z \rangle$, $\Delta S_{f_l}^z = S_{f_l}^z - R_l$, $\theta_{l,l+1} = \theta_l - \theta_{l+1}$, the angular brackets $\langle \ldots \rangle$ imply the thermal averaging, the sublattice index l is defined modulo 3 (e.g., indices $l = 4$ and 5 correspond to the first and second sublattices, respectively), and N is the number of lattice sites.

The angles θ_l are determined from the solution of the set of three equations ($l = 1, 2, 3$)

$$3I(R_{l+1} \sin\theta_{l,l+1} - R_{l+2} \sin\theta_{l+2,l}) = gH \sin\theta_l, \quad (6)$$

which are obtained from the condition of vanishing of the coefficients of the terms that arise in the Hamiltonian $\mathcal{H}_m$ after the unitary transformation and include only one $S_{f_l}^x$ operator. This ensures that, in the mean-field approximation (i.e., neglecting $\mathcal{H}_{\text{int}}$), we have for all averages $\langle S_{f_l}^x \rangle = 0$ and all vectors $\mathbf{R}_l$ are directed along the new z_l axes.

Indeed, only two of three equations (6) are linearly independent. Having in mind only nontrivial solutions, we can write these two equations in the form

$$\sum_{l=1}^{3} R_l \sin\theta_l = 0, \quad \sum_{l=1}^{3} R_l \cos\theta_l = \frac{gH}{3I}. \qquad (7)$$

From the first equation, it follows that the total magnetic moment of the system in the mean-field approximation is always directed strictly along the applied magnetic field. The second equation determines the total magnetic moment as a function of the applied magnetic field.

The existence of only two equations (7) determining three angles θ_l implies a high degree of degeneracy in the mean-field approximation. In [3, 4], it was shown that such degeneracy is lifted by quantum fluctuations. Hence, at low temperatures, the third equation for the angles is that obtained by the minimization of the thermal average of Hamiltonian (3) involving $\mathcal{H}_{\rm int}$. The value of $\langle\mathcal{H}_{\rm int}\rangle$ is mainly determined by such pair averages, which do not contain the operator $\Delta S^z_{f_l}$. To calculate these averages and the values of R_l, we introduce the Matsubara Green's functions

$$D^{(l,l')}_{\alpha\beta}(f_l - f_{l'}, \tau - \tau') = -\langle T_\tau \tilde{S}^{\alpha}_{f_l}(\tau)\tilde{S}^{\overline{\beta}}_{f_{l'}}(\tau')\rangle, \qquad (8)$$

where T_τ is the ordering operator over the imaginary time τ, l and l' are the numbers of magnetic sublattices, α and β take the values $\pm$, $\overline{\beta} = -\beta$, and $\tilde{S}^{\alpha}_{f_l}(\tau)$ operators are specified in the Heisenberg representation as $\tilde{S}^{\alpha}_{f_l}(\tau) = e^{\tau\mathcal{H}'_m} S^{\alpha}_{f_l} e^{-\tau\mathcal{H}'_m}$.

Green's functions (8) are calculated using the diagram technique for spin operators [18, 19] with the operator $\mathcal{H}_{\rm int}$ playing the role of the perturbation Hamiltonian. In the zero-loop approximation, the set of equations for the Green's functions has the graphical form

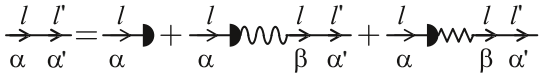

(9)

Here, the thick line with the double arrow corresponds to the Fourier transform $D^{(l,l')}_{\alpha\beta}(k, i\omega_n)$ of the Green's function (8), where k is the crystal momentum and $\omega_n = 2n\pi T$ is the even Matsubara frequency ($n \in Z$). The thin line with the arrow denotes the unrenormalized propagator $g^{(l,l')}_{\alpha}(i\omega_n) = \delta_{ll'}/(i\omega_n + \alpha H_l)$, where $\delta_{ll'}$ is the Kronecker delta. In the approximation under discussion, the terminal factor (closed semicircle in Eq. (9)) equals $2R_l$. The wavy line corresponds to the interaction between spins within the same triangular lattice

$$V^{(l,l')}_{\alpha\beta}(k) = \alpha I \gamma(\pm k)(\cos\theta_{ll'} + \alpha\cdot\beta\cdot 1)/4, \qquad (10)$$

where

$$\gamma(k) = 2\cos(k_x/2)\exp(ik_y/2\sqrt{3}) + \exp(-ik_y/\sqrt{3}),$$

k_x and k_y are specified in units of the lattice constant, and $\gamma(+k)$ and $\gamma(-k)$ are taken if $l' = l + 1$ and $l + 2$ (mod 3), respectively. The sawtooth curve in (9) corresponds to the interaction between the nearest neighbor spins from different triangular lattices: $V^{\perp}_{\alpha}(k) = \alpha 2 I_{\perp}\cos k_z$. In (9), the summation over β is implied.

The condition of consistency of system (9) gives us three branches in the spectrum of spin-wave excitations, two of them being gapless. The first gapless branch (Goldstone mode) is a linear function of the crystal momentum k near the center of the Brillouin zone. The second gapless branch is quadratic in k and ensures the absence of the long-range magnetic order at any nonzero temperature in the purely two-dimensional isotropic AFTL. The weak ferromagnetic coupling between the triangular lattices stabilizes the long-range magnetic order at nonzero temperatures T.

Expressing the Green's functions given by Eq. (8) from system (9) in the conventional way, we obtain the equations for the average vales of R_l ($l = 1, 2, 3$) and the expressions for the pair correlation functions $\langle S^{\alpha}_{f_l} S^{\alpha'}_{f_{l'}}\rangle$. The latter are used in calculations of $\langle\mathcal{H}'_m\rangle$. The minimization of $\mathcal{H}'_m$ (at low temperatures T) gives us the third (in addition to Eqs. (7)) equation for the angles θ_l ($l = 1, 2, 3$). We do not present here the lengthy explicit form of the system of six equations for R_l and θ_l.

The numerical calculations demonstrate that the nontrivial solutions (for which all angles θ_l are not multiples of π) always satisfy the conditions $|\theta_3| = \theta_1$ and $R_3 = R_1$ (see Fig. 1). In this case, $\theta_3 = -\theta_1$ in the Y phase (then, $\theta_2 = \pi$) and $\theta_3 = \theta_1$ in the V phase. The collinear solution (*uud* phase) arises only at one applied magnetic field $H = H_{\rm sat}/3$.

3. MAGNETIZATION OF THE QUANTUM ANTIFERROMAGNET ON THE TRIANGULAR LATTICE TAKING INTO ACCOUNT QUANTUM FLUCTUATIONS

The stabilization of the *uud* phase within a finite magnetic field range can be achieved by taking into account the quantum fluctuation corrections for the canting angles between the magnetization of the sublattices. The type of magnetic structure (or phase) is now determined by the canting angles $\tilde{\theta}_l (l = 1, 2, 3)$ calculated involving such corrections. These angles

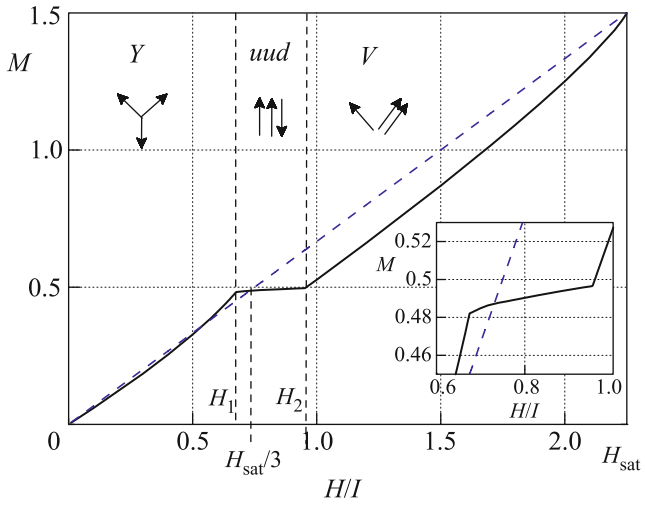

Fig. 2. (Color online) Magnetic field dependence of the magnetization for the quasi-two-dimensional Heisenberg model on the triangular lattice in the (dashed line) mean-field and (solid line) zero-loop approximations. The parameters of the model are $I_z/I = 0.1$ and $T/I = 10^{-5}$. The inset shows the magnetic field range with the magnetization plateau on a magnified scale.

can be found by minimizing the thermodynamic potential $\Omega(T) = -T \ln\{e^{-\mathcal{H}_m/T}\}$

$$\frac{gH}{3I} R_l \sin\tilde{\theta}_l = (R_l R_{l+1} + C_{l,l+1}) \sin\tilde{\theta}_{l,l+1} + (R_l R_{l+2} + C_{l,l+2}) \sin\tilde{\theta}_{l,l+2}, \quad (11)$$

where, as before, $\tilde{\theta}_{l,l'} = \tilde{\theta}_l - \tilde{\theta}_{l'}$ and the sublattice indices l are defined modulo 3. The quantum fluctuations in Eqs. (11) manifest themselves via the correlation functions $C_{l,l'} = \langle S^x_{f_l} S^x_{f_{l'}} \rangle$. At $C_{l,l'} = 0$, Eqs. (11) are reduced to Eqs. (6).

The sum of three equations (11) yields $\sum_{l=1}^{3} R_l \sin\tilde{\theta}_l = 0$. This means that the transverse magnetization still vanishes at all values of the applied magnetic field even taking into account quantum fluctuations. This result is in contrast to the conclusions reported in [3], where a nonzero transverse magnetization was found in the V phase.

The expressions describing the magnetic field dependence of the longitudinal magnetization $M = \sum_{l=1}^{3} R_l \cos\tilde{\theta}_l$ follow from equations (11). For the three phases Y, uud, and V, they can be written in the form

$$M_Y = \frac{R_1 C_{12} - R_2 C_{13} + R_1^2 gH/3I}{R_1^2 + C_{13}},$$
$$M_{uud} = 2R_1 - R_2, \quad M_V = \frac{gH/3I}{1 + C_{12}/R_1 R_2}, \quad (12)$$

where it is taken into account that $C_{12} = C_{23}$.

The analysis of Eqs. (11) and (12) demonstrates that an increase in the applied magnetic field from zero value results in the transition of the Y phase to the collinear uud phase at the magnetic field H_1 lower than $H_{sat}/3$ (see Fig. 2). Similarly, with a decrease in the applied magnetic field from H_{sat}, the noncollinear V phase is transformed to the uud phase at $H_2 > H_{sat}/3$. In the magnetic field range from H_1 to H_2, Eqs. (11) have only trivial solutions corresponding to the uud phase. As demonstrated within the spin-wave theory at $T = 0$ [3, 4, 20], the magnetic field dependence of the magnetization in this phase is described by the strictly horizontal segment with $M = M_{sat}/3$. In our approach, the $M(H)$ curve has a slight slope between H_1 and H_2 clearly seen in the inset of Fig. 2.

4. HAMILTONIAN OF AN AFTL SEMIMETAL

Now, passing to the main aim of our work, we note that the drastic change in the $M(H)$ dependence at the points H_1 and H_2 should manifest itself in the characteristics of itinerant electrons under the condition that their coupling with the localized spins is strong enough. To study such manifestations, let us add charge carriers (electrons and holes) to the magnetic system discussed above. The motion of these charge carriers should be bounded within the limits of triangular lattices and they should interact with the localized spins by the strong s–$d(f)$ exchange coupling. We also assume that electron and hole bands slightly overlap, thus forming a semimetal with a low charge carrier density. The Hamiltonian of such AFTL semimetal in the applied magnetic field has the form

$$\mathcal{H} = \mathcal{H}_m + \mathcal{H}_c + \mathcal{H}_J. \quad (13)$$

The operator $\mathcal{H}_m$ is defined by Eq. (1).

The term $\mathcal{H}_c$ in (13) is the energy operator for charge carriers

$$\mathcal{H}_c = \sum_{ij\lambda\sigma} ((\varepsilon_\lambda - \mu_\lambda)\delta_{ij} + t_{ij}^{\lambda}) c^+_{i\lambda\sigma} c_{j\lambda\sigma} + 2H \sum_j \sigma^z_{j\lambda}. \quad (14)$$

Here, $c^+_{j\lambda\sigma}$ and $c_{j\lambda\sigma}$ are the creation and annihilation operators for an electron ($\lambda = e$) or hole ($\lambda = h$) with the spin projection $\sigma = \pm 1/2$ at the jth site, respectively; ε_λ and μ_λ are the binding energy and chemical potential for the particles of kind λ, respectively; $\mu_e = \mu$, and $\mu_h = -\mu$; t_{ij}^{λ} is the tunneling integral, which is nonzero only for hoppings between the nearest neighbor sites within the same triangular lattice and is equal to t^{λ}; and $\sigma^z_{j\lambda}$ is the operator for the z projection of the spin for a quasiparticle of kind λ at the jth site.

The third term in Eq. (13) corresponds to the s–$d(f)$ exchange interaction with the magnitude J^λ between the localized and itinerant subsystems

$$\mathcal{H}_J = \sum_{j\lambda} J^\lambda \mathbf{S}_j \boldsymbol{\sigma}_{j\lambda}, \tag{15}$$

where $\boldsymbol{\sigma}_{j\lambda}$ is the vector spin operator of the quasiparticle of kind λ at the jth site.

Owing to the locality of the s–$d(f)$ exchange interaction, the operator $\mathcal{H}_J$ is invariant under the aforementioned unitary transformation corresponding to the transition between the local coordinate systems.

As before, we divide the system into three sublattices and pass to the local coordinate systems, performing the unitary transformation of the operator $\mathcal{H}_c$. In this case, the transformation for the c-operators has the form

$$c_{fj\lambda\sigma}(\tilde{\theta}_l) = c_{fj\lambda\sigma}\cos\tilde{\theta}_l/2 + 2\bar{\sigma}c_{fj\lambda\bar{\sigma}}\sin\tilde{\theta}_l/2, \tag{16}$$

where the rotation angles $\tilde{\theta}_l$ are determined only by the dynamics of localized spins and are calculated taking into account quantum fluctuations. Then, we add the mean-field contribution from the operator $\mathcal{H}_J$ to the transformed Hamiltonian $\mathcal{H}'_c$ and pass to the k representation. As a result, we obtain the Hamiltonian for the itinerant subsystem

$$\begin{aligned}\mathcal{H}_{eh} = \sum_{kl\lambda\sigma}\Bigg[&(\varepsilon_\lambda - \mu_\lambda - \sigma\bar{H}_l)c^+_{kl\lambda\sigma}c_{kl\lambda\sigma} + h_l c^+_{kl\lambda\sigma}c_{kl\lambda\bar{\sigma}} \\ &+ \cos\frac{\tilde{\theta}_{l,l+1}}{2}\left(t^\lambda_k c^+_{kl\lambda\sigma}c_{k,l+1,\lambda\sigma} + \text{H.c.}\right) \\ &+ 2\sigma\sin\frac{\tilde{\theta}_{l,l+1}}{2}\left(t^\lambda_k c^+_{kl\lambda\sigma}c_{k,l+1,\lambda\bar{\sigma}} + \text{H.c.}\right)\Bigg].\end{aligned} \tag{17}$$

Here, $\bar{H}_l = JR_l + 2H\cos\tilde{\theta}_l$, $h_l = H\sin\tilde{\theta}_l$, and $t^\lambda_k = t^\lambda\gamma(k)$. In the notation of the c-operator, we add the lattice index l, which is as before defined modulo 3.

5. ENERGY SPECTRUM OF CHARGE CARRIERS

The dispersion equation determining six branches of the fermion spectrum of charge carriers follows from the condition of vanishing of the determinant for the set of equations of motion for the c-operators $i\dot{c}_{kl\lambda\sigma} = [c_{kl\lambda\sigma}, \mathcal{H}_{eh}]$. This equation has the form

$$\begin{vmatrix} A_1(\omega) & B_{12}(k) & B_{31}(k)^* \\ B_{12}(k)^* & A_2(\omega) & B_{23}(k) \\ B_{31}(k) & B_{23}(k)^* & A_3(\omega) \end{vmatrix} = 0, \tag{18}$$

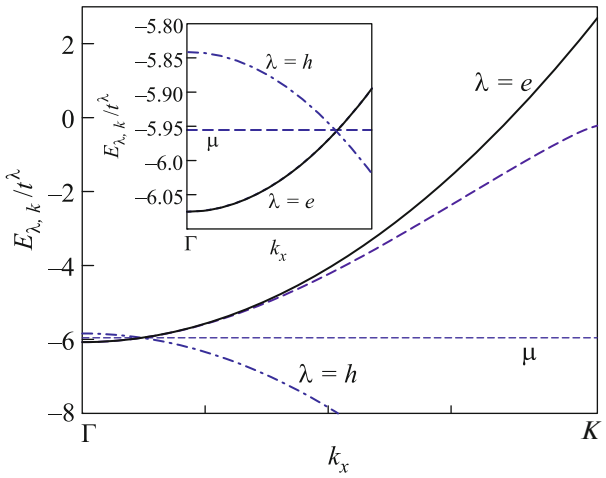

Fig. 3. (Color online) Lower branches of the spectrum of electronic states ($\lambda = e$) calculated (thick dashed line) from the dispersion equation (18) and (solid line) in the effective mass approximation. The dot-dashed line corresponds to the spectrum of hole states ($\lambda = h$) in the valence band. The position of the chemical potential μ is shown by the thin dashed line. The inset shows on a magnified scale the vicinity of the Γ point of the Brillouin zone at the level of μ. The parameters of the model (in electronvolts) are $t^e = t^h = -1$, $J^e = J^h = 1$, $I = 0.004$, and $H = 2.4\times10^{-3}$. In the Brillouin zone, the Γ and K points have the coordinates $(0,0)$ and $(\pi,0)$, respectively.

where

$$\begin{aligned} A_l(\omega) &= \begin{pmatrix} \omega - \varepsilon_\lambda + \mu_\lambda & -\sigma\bar{H}_l - ih_l \\ -\sigma\bar{H}_l + ih_l & \omega - \varepsilon_\lambda + \mu_\lambda \end{pmatrix}, \\ B_{ll'}(k) &= -t^\lambda_k \begin{pmatrix} e^{i\sigma\tilde{\theta}_{ll'}} & 0 \\ 0 & e^{-i\sigma\tilde{\theta}_{ll'}} \end{pmatrix}, \end{aligned} \tag{19}$$

$l, l' = 1, 2, 3$.

The calculations show that two lower spectral branches are degenerate at $H = 0$ and become split at nonzero magnetic field. In the regime of a low charge carrier density, these branches can be represented by an approximate expression quadratic in k: $E_{\lambda k} = \hbar^2k^2/2m^*_\lambda$. The effective mass m^*_λ can be found from the analysis of Eq. (18) at low k values. We do not present the lengthy expression for m^*_λ. However, in Fig. 3, we illustrate the high accuracy of the effective mass approximation in the description of the fermion spectrum near the Γ point of the Brillouin zone.

In Fig. 3, we can see that the spectra calculated using Eq. (18) nearly coincide with those corresponding to the effective mass approximation within a half of the Brillouin zone. In the plots of electron and hole spectral branches, the parameters $\varepsilon_{e(h)}$ and chemical potential μ are chosen according to the conditions of the electron–hole compensation and the low charge

carrier density, $\sim 10^{20}$ cm^{-3}. The effective mass m_λ^* turns out to be equal to the free electron mass if the lattice constant of the triangular lattice equals $a = 3.5 \times 10^{-8}$ cm at the model parameters specified in Fig. 3. At the chosen magnitude of the exchange interaction ($I = 0.004$ eV), the magnetic field $H = 2.4 \times 10^{-3}$ eV corresponds to the left part of the left edge of the magnetization plateau for the localized subsystem (see Fig. 2). At such value of the applied magnetic field, the splitting of the lower spectral branches of the fermion spectrum degenerate at $H = 0$ is so large that only one lower branch turns out to be occupied.

6. QUANTUM OSCILLATIONS OF MAGNETIZATION IN AFTL SEMIMETALS

In [16], it is demonstrated that the change in the magnetic moment of the localized spins for antiferromagnetic semimetals with the square lattice induced by an increase in the applied magnetic field can lead to the displacement of the bottom of the conduction band and the top of the valence band related to the strong s–$d(f)$ exchange coupling. Under the condition of the electron–hole compensation giving rise to the pinning of the chemical potential, this can provide an additional mechanism (along with the conventional one) of the motion of Landau levels with respect to μ and, hence, it can change the frequency of de Haas–van Alphen oscillations within the magnetic field range where the form of $M(H)$ changes drastically. In [16], this field corresponds to the spin-flip transition. In the case of the AFTL metal under discussion, the drastic change in $M(H)$ is observed not only at the spin-flip transition point but also at the points H_1 and H_2 (see Fig. 2). Thus, an anomalous behavior of the de Haas–van Alphen effect in an AFTL semimetal can be expected at these values of the applied magnetic field.

To check this conjecture, we calculate the magnetization oscillations for the itinerant subsystem using the Lifshitz–Kosevich formula tor the two-dimensional electron gas:

$$M_\sim = A\sum_{n=1}^{+\infty} \frac{(-1)^n \cos\left(\frac{m_\lambda^*}{m}\pi n\right)\sin\left(\frac{2\pi\tilde{\mu}}{\hbar\omega_H}n\right)}{\sinh\left(\frac{2\pi^2 T}{\hbar\omega_H}n\right)}, \qquad (20)$$

where $\tilde{\mu}$ is the Fermi energy, $\omega_H = eH/m_\lambda^* c$ is the cyclotron frequency, and m is the free electron mass. The oscillation amplitude disregarding the scattering processes can be written in the form $A = -2T\tilde{\mu}m_\lambda^*\mu_B/\hbar^2 H a_z$, where μ_B is the Bohr magneton and $a_z = 6 \times 10^{-8}$ cm is the distance between the triangular planes. For simplicity, the parameters of electron and hole subbands are chosen to be the same (see the caption of Fig. 3).

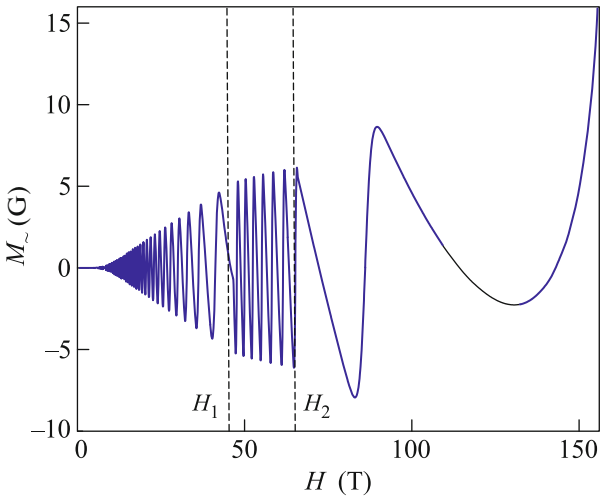

Fig. 4. (Color online) Quantum oscillations of the magnetization of AFTL semimetal. The parameters of the model are the same as in Figs. 2 and 3.

The magnetization $M_\sim$ calculated by Eq. (20) is shown in Fig. 4. As expected, a drastic change in the frequency of magnetization oscillations for the itinerant subsystem is indeed observed near H_1 and H_2.

7. CONCLUSIONS

In conclusion, we note an important role of quantum fluctuations and the s–$d(f)$ exchange coupling in the observation of $M_\sim$ anomalies shown in Fig. 4. The quantum fluctuations are responsible for the plateau in the magnetization of localized spins, whereas the s–$d(f)$ exchange coupling provides an additional mechanism for the motion of Landau levels under the effect of the applied magnetic field.

Note also that the diagram technique used in our work is developed to describe the characteristics of quantum magnets at nonzero temperatures. However, the calculations of both M and $M_\sim$ have been performed for sufficiently low temperature $T/I = 10^{-5}$. Therefore, for the selection of accidentally degenerate levels, it is sufficient to minimize the energy (the average of the Hamiltonian). It is apparent that, at higher temperatures, we should minimize the free energy. In this connection, it is noteworthy that the H–T phase diagram for $CsCuCl_3$ was recently constructed in [21]. The corresponding model for this substance differs from model (1), first, in the existence of anisotropy Δ in the interplane exchange interaction and, second, in the ratio of the exchange parameters $|I_\perp| \gg I$ (in our case, $|I_\perp| \ll I$). At $\Delta = 0$, the low-temperature region of the H–T phase diagram obtained in [21] in the spin-wave approximation is in good agreement with results

of our diagram calculations. The explicit form of $M(H)$ is not reported in [21]; therefore, it is impossible to check our conclusion concerning a slight slope of the $M(H)$ curve in the magnetic field range where the strictly horizontal plateau with $M = M_{sat}/3$ in the magnetization of localized spins is expected (see Fig. 2). The slight positive slope of $M(H)$ obtained in this work is related to the zero-loop approximation used in the diagram technique to explicitly take into account the effects of quantum spin reduction.

Finally, we note that the low charge carrier density allows us not only to justify the effective mass approximation in the calculations of $M_{\sim}$ but also to take into account only quantum fluctuations in the choice of degenerate configurations in the subsystem of localized spins. At a significant doping level in the presence of the s–$d(f)$ exchange coupling, the effect of the itinerant subsystem can itself (even without quantum fluctuations) ensure the lifting of degeneracy in the localized subsystem.

We are grateful to Prof. V.V. Val'kov for helpful discussions and valuable remarks. This work was supported by the Russian Foundation for Basic Research, project nos. 16-02-00073 and 18-02-00837.

REFERENCES

1. R. S. Gekht, Sov. Phys. Usp. **32**, 871 (1989).
2. H. Kawamura and S. Miyashita, J. Phys. Soc. Jpn. **54**, 4530 (1985).
3. D. I. Golosov and A. V. Chubukov, JETP Lett. **50**, 451 (1989).
4. A. V. Chubukov and D. I. Golosov, J. Phys.: Condens. Matter **3**, 69 (1991).
5. H. Kitazawa, H. Suzuki, H. Abe, J. Tang, and G. Kido, Phys. B (Amsterdam, Neth.) **259–261,** 890 (1999).
6. L. E. Svistov, A. I. Smirnov, L. A. Prozorova, O. A. Petrenko, A. Micheler, N. Büttgen, A. Ya. Shapiro, and L. N. Demianets, Phys. Rev. B **74**, 024412 (2006).
7. A. I. Smirnov, H. Yashiro, S. Kimura, M. Hagiwara, Y. Narumi, K. Kindo, A. Kikkawa, K. Katsumata, A. Ya. Shapiro, and L. N. Demianets, Phys. Rev. B **75**, 134412 (2007).
8. Y. Shirata, H. Tanaka, A. Matsuo, and K. Kindo, Phys. Rev. Lett. **108**, 057205 (2012).
9. R. Ishii, S. Tanaka, K. Onuma, Y. Nambu, M. Tokunaga, T. Sakakibara, N. Kawashima, Y. Maeno, C. Broholm, D. P. Gautreaux, J. Y. Chan, and S. Nakatsuji, Eur. Phys. Lett. **94**, 17001 (2011).
10. M. Ogata, J. Phys. Soc. Jpn. **72**, 1839 (2003).
11. G. Baskaran, Phys. Rev. Lett. **91**, 097003 (2003).
12. Y. Kobayashi, M. Yokoi, and M. Sato, J. Phys. Soc. Jpn. **72**, 2453 (2003).
13. M. M. Korshunov and I. Eremin, Phys. Rev. B **77**, 064510 (2008).
14. V. V. Val'kov and A. O. Zlotnikov, JETP Lett. **104**, 483 (2016).
15. J. M. Ok, Y. J. Jo, K. Kim, T. Shishidou, E. S. Choi, Han-Jin Noh, T. Oguchi, B. I. Min, and J. S. Kim, Phys. Rev. Lett. **111**, 176405 (2013).
16. V. V. Val'kov and D. M. Dzebisashvili, Phys. Solid State **39**, 179 (1997).
17. D. M. Dzebisashvili and A. A. Khudaiberdyev, Phys. Solid State **58**, 1071 (2016).
18. R. O. Zaitsev, Sov. Phys. JETP **41**, 100 (1975).
19. V. V. Val'kov and S. G. Ovchinnikov, *Quasiparticles in Strongly Correlated Systems* (Sib. Otdel. RAN, Novosibirsk, 2001) [in Russian].
20. T. Coletta, T. A. Toth, K. Penc, and F. Mila, Phys. Rev. B **94**, 075136 (2016).
21. M. Hosoi, H. Matsuura, and M. Ogata, J. Phys. Soc. Jpn. **87**, 075001 (2018).

Translated by K. Kugel